

PRECISION MASS DETERMINATION OF THE HIGGS BOSON AT PHOTON-PHOTON COLLIDERS*

TOMOMI OHGAKI

*Lawrence Berkeley National Laboratory
Berkeley, California 94720, USA*

We demonstrate a measurement of the Higgs boson mass by the method of energy scanning at photon-photon colliders, using the high energy edge of the photon spectrum. With an integrated luminosity of 50 fb^{-1} it is possible to measure the standard model Higgs mass to within 110 MeV in photon-photon collisions for $m_h = 100 \text{ GeV}$. As for the total width of the Higgs boson, the statistical error $\Delta\Gamma_h/\Gamma_{h \text{ SM}} = 0.06$ is expected for $m_h = 100 \text{ GeV}$, if both $\Gamma(h \rightarrow \gamma\gamma)$ and $\Gamma(h \rightarrow b\bar{b})$ are fixed at the predicted standard model value.

1. Introduction

One of the most important tasks of the current and future collider experiments will be to detect and study Higgs boson(s). The accuracy of the measurement of the Higgs boson mass will impact precision tests of loop corrections, both in the standard model (SM) and in the extended models such as the minimal supersymmetric model (MSSM).^{1,2,3} Deviations of the total widths of the Higgs bosons from SM predictions can be directly compared to predictions of alternative models such as the MSSM, the non-minimal supersymmetric standard model, or the general two-Higgs-doublet model.^{1,2,3} The total widths for the SM Higgs boson h_{SM} and the three neutral Higgs bosons h^0, H^0, A^0 of the MSSM are shown in Fig. 1.

The interaction of high energy photons at a photon-photon collider^{4,5,6} provides us with an unique opportunity to study Higgs boson, because the SM Higgs boson in s -channel resonance can be produced at photon-photon colliders.^{7,8,9,10,11} In this paper we point out precision measurements of mass (m_h) and total width (Γ_h) of the Higgs boson by the method of energy scanning, using the high energy edge of the photon spectrum.

The method of energy scanning at photon-photon colliders was first mentioned by V. Telnov.⁶ The luminosity of the photon-photon collider has a very sharp edge at high energy, much narrower than the width of the luminosity peak. If the Higgs boson is a very narrow resonance, we will observe a rapid increase in the visible cross section of the Higgs production during energy scanning.

*This work was supported in part by the U.S. Department of Energy under Contract No. DE-AC03-76SF00098.

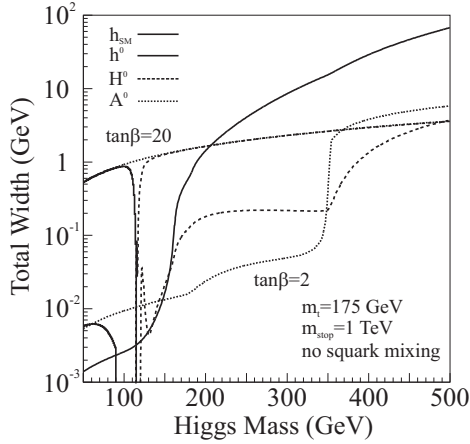


Fig. 1. The total widths of the SM and MSSM Higgs bosons. The top quark mass is assumed to be 175 GeV. In the case of the MSSM, the results for $\tan\beta = 2$ and 20 are shown, taking $m_{\tilde{t}} = 1$ TeV, including two-loop radiative corrections, and neglecting squark mixing. SUSY decay channels are assumed to be absent. Computed by HDECAY.¹⁶

2. Luminosity of Photon-Photon Colliders

Figure 2 shows ten differential luminosities with the $J_z = 0$ angular momentum state of initial photon collisions in a photon-photon collider for energy scanning at $m_h = 100$ GeV. In this study, we have scanned the Higgs boson resonance from the left side to the right side in Fig. 2. The circles exhibit the luminosity points in contact with the Higgs boson and the rise of the luminosity at $m_h = 100$ GeV is rapid at the threshold of energy scanning. Here we introduce the required parameters for the luminosity calculation. A laser photon of energy ω_L is scattered by an electron beam of energy E_e in the conversion region of the photon-photon collider. The kinematics of Compton scattering is characterized by the dimensionless parameter⁴

$$x \equiv \frac{4E_e\omega_L}{m_e^2} \approx 15.3 \left[\frac{E_e}{\text{TeV}} \right] \left[\frac{\omega_L}{\text{eV}} \right], \quad (1)$$

where m_e is electron mass. The maximum energy of the scattered photon ω_{max} is $E_e x / (x + 1)$ given by x . The parameter x is fixed to be 4.8, and we get $\omega_{max} = 100$ GeV when $E_e = 121$ GeV and $\omega_L = 2.6$ eV. The combination of the polarizations of the electron P_e and the laser P_L should be $P_L P_e = -1$ so that the generated photon spectrum peaks at its maximum energy.

The differential luminosity distribution depends on the variable $\rho = b/(\gamma a)$, where a is the rms radius of the electron beam at the interaction point (IP), b is the distance between the conversion point (CP) and the IP, and $\gamma = E_e/m_e$. The polarized luminosities with the $J_z = 0$ and the $J_z = \pm 2$ in a photon-photon collider were used in Ref. 4. Here we assumed $\rho = 1$ and the conversion coefficient $k = 0.6$. It should be noted that the shape of the high energy edge and w_{max} are influenced

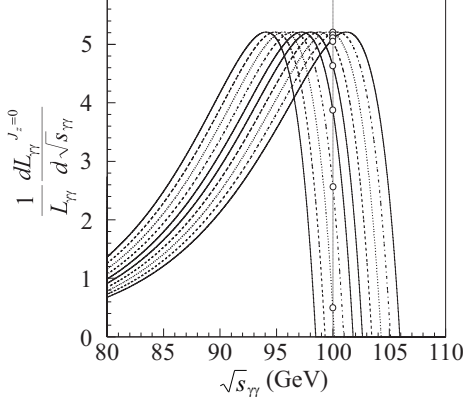


Fig. 2. Ten differential luminosities with $J_z = 0$ as a function of the center-of-mass energy in a photon-photon collider for energy scanning at $m_h = 100$ GeV.

by nonlinear effects due to very strong focus of the laser field at the CP. Prior to the actual energy scan, we need to have a fairly good estimate for nonlinear effects including the polarization.

3. Higgs Boson and Backgrounds

Once the Higgs boson is observed at future e^+e^- colliders, we must determine its precise mass and width in order to reveal the fundamental properties of the Higgs boson. At a photon-photon collider, the feasibility of the measurement of the two-photon decay width of a Higgs boson has been studied in the mass range $M_W < m_h < 2M_W$.^{7,8,9,10,11} For $m_h < 2M_W$, the SM Higgs boson mainly decays into a $b\bar{b}$ pair and the daughter b -flavored hadrons will be easily identified due to their long lifetime; therefore, the $b\bar{b}$ events are the best signals. The cross section of the Higgs boson production can be described by the Breit-Wigner approximation:

$$\sigma_{\gamma\gamma \rightarrow h \rightarrow b\bar{b}}(\sqrt{s}) = 8\pi \frac{\Gamma(h \rightarrow \gamma\gamma)\Gamma(h \rightarrow b\bar{b})}{(s - m_h^2)^2 + m_h^2\Gamma_h^2} (1 + \lambda_1\lambda_2), \quad (2)$$

where $\Gamma(h \rightarrow \gamma\gamma)$ and $\Gamma(h \rightarrow b\bar{b})$ are the decay widths of the Higgs boson into two photons and a $b\bar{b}$ pair, λ_1 and λ_2 the initial photon helicities, respectively. The effective cross section of the signal events within $m_h - \delta < \sqrt{s} < m_h + \delta$ is

$$\sigma_{\gamma\gamma \rightarrow h \rightarrow b\bar{b}}^{\text{eff}} = \int_{m_h - \delta}^{m_h + \delta} 16\pi \frac{\Gamma(h \rightarrow \gamma\gamma)\Gamma(h \rightarrow b\bar{b})}{(\hat{s} - m_h^2)^2 + m_h^2\Gamma_h^2} \frac{1}{L_{\gamma\gamma}} \frac{dL_{\gamma\gamma}^{J_z=0}}{d\sqrt{\hat{s}}} d\sqrt{\hat{s}}, \quad (3)$$

where δ expresses the effect of the detector resolution and we assumed $\delta = 5$ GeV. Here we supposed that the total luminosity is $L_{\gamma\gamma} = L_{\gamma\gamma}^{J_z=0} + L_{\gamma\gamma}^{J_z=\pm 2}$.

The main background processes may be the continuum $\gamma\gamma \rightarrow b\bar{b}$, $c\bar{c}$ as well as the radiative processes $\gamma\gamma \rightarrow b\bar{b}g$, $c\bar{c}g$. The continuum backgrounds dominantly

produced by initial photon collisions in the $J_z = \pm 2$ can be suppressed by controlling the polarization of the colliding photon beams. Several authors reported that the effect of QCD corrections to $\gamma\gamma \rightarrow q\bar{q}$ is large since the helicity suppression which affects the background $q\bar{q}$ events does not work due to a gluon emission.^{9,10} Recently leading double-logarithmic QCD corrections for $J_z = 0$ were resummed to all orders and the account of non-Sudakov form factor to higher orders makes the cross-section well defined and positive definite in all regions of the phase space.¹² In this study we take account of the one-loop QCD corrections of the soft gluon emission, hard gluon emission, and virtual correction, where higher order double logarithmic corrections are not taken into account.¹⁰ The effective cross section of the background process $\gamma\gamma \rightarrow b\bar{b}(g)$ or $c\bar{c}(g)$ within $m_h - \delta < \sqrt{s} < m_h + \delta$ is

$$\sigma_{\text{bg}}^{\text{eff}} = \int_{m_h - \delta}^{m_h + \delta} \sigma_{\text{bg}}(\sqrt{\hat{s}}) \frac{1}{L_{\gamma\gamma}} \frac{dL_{\gamma\gamma}}{d\sqrt{\hat{s}}} d\sqrt{\hat{s}}, \quad (4)$$

where $\sigma_{\text{bg}}(\sqrt{s})$ is the cross section of the background process.

Since the cross section of $\gamma\gamma \rightarrow c\bar{c}$ is larger than that of $\gamma\gamma \rightarrow b\bar{b}$ due to the large electric charge of the quark, we apply the b tagging in order to eliminate the charm and the light quark backgrounds. By the topological vertexing method¹³ and the LC Vertex Detector design,¹⁴ the efficiency and purity of b -quark jet identification are 70% and 99%, respectively. Therefore the tagging efficiencies of $b\bar{b}(g)$ and $c\bar{c}(g)$ events are assumed as 49% and 0.005% with double tagging, respectively.^a¹⁵ We impose the following cuts to remove backgrounds: (1) the double $b\bar{b}$ tagging in the event; (2) $|\cos \theta_{b,\bar{b}}| < 0.95$, where $\theta_{b,\bar{b}}$ is the scattering angle of the $b(\bar{b})$ quark; (3) $|M_{b\bar{b}} - m_h| < 5$ GeV.

4. Results and Discussion

Figure 3 shows an example of energy scan to determine m_h . Each energy point corresponds to 5 fb^{-1} and the total luminosity of photon-photon collisions is 50 fb^{-1} in the same distributions as with Fig. 2. The total width of the SM Higgs boson Γ_h for $m_h = 100$ GeV is 2.16 MeV, which is computed by the HDECAY program.¹⁶ The partial widths $\Gamma(h \rightarrow \gamma\gamma)$ and $\Gamma(h \rightarrow b\bar{b})$ at the predicted SM value with $m_h = 100$ GeV are fixed for energy scanning at $m_h = 99.8, 100, 100.2$ GeV. The statistical errors in Fig. 3 indicate $\sqrt{S + B}$, where S and B are the numbers for signal and background events. From Fig. 3, we can understand that the method of energy scanning for m_h is more effective than that of the measurement of a single point at the luminosity peak using the same total luminosity, because the statistical errors at the threshold of energy scanning are smaller than that at the luminosity peak and we can distinguish the mass difference of 200 MeV. With the energy scanning of 10 points, the attainable error in m_h is about 110 MeV at the 1σ level.

^aThe interaction region (IR) at photon-photon colliders is complicated, because there are the sweeping magnet for spent electrons and the optical mirror system for laser focusing around the vertex detector. We need to study the performance of the vertex detector at the IR.

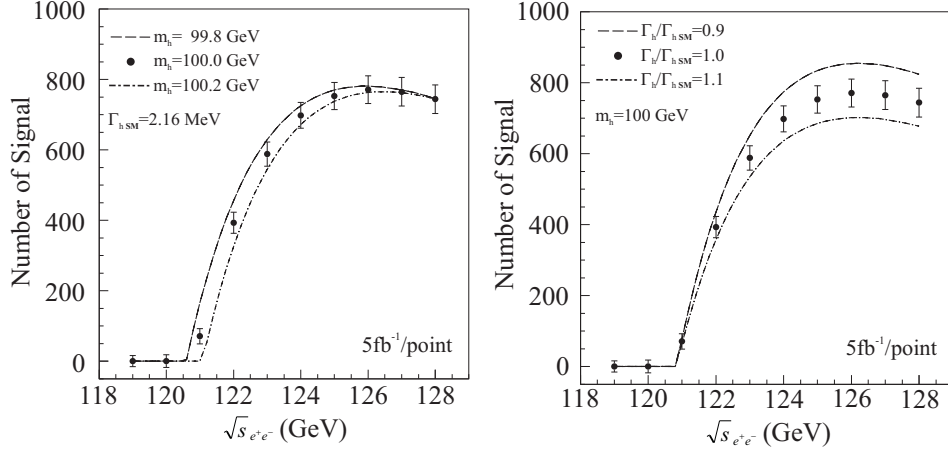


Fig. 3. An example of energy scan to determine m_h where each point corresponds to 5 fb^{-1} .

Fig. 4. An example of energy scan to determine Γ_h where each point corresponds to 5 fb^{-1} .

The measurement for the determination of Γ_h by the method of energy scan is shown in Fig. 4. Each energy point corresponds to 5 fb^{-1} and the total luminosity is 50 fb^{-1} . The partial widths $\Gamma(h \rightarrow \gamma\gamma)$ and $\Gamma(h \rightarrow b\bar{b})$ at the predicted SM value with $m_h = 100 \text{ GeV}$ are fixed for energy scanning $\Gamma_h/\Gamma_{h\text{SM}} = 0.9, 1.0, 1.1$. The large difference between the total widths at the luminosity peak can be seen easily in Fig. 4. The statistical error in Γ_h is about 6% at the 1σ level. If there are additional invisible decay modes of Higgs boson, only the total decay width increases keeping the partial widths of two photons and a $b\bar{b}$ pair unchanged. In this study we find $\Gamma_h/\Gamma_{h\text{SM}} > 1$. Of course, this deviation from the SM should have also been observed in the parent e^+e^- collider. However, this will be independent observation in gamma-gamma energy scan, which confirms the e^+e^- result.

Here we consider two cases for the photon-photon collider. First, we choose $x = 4.8$ while tuning the energies of the laser photon and the electron beam while tuning the scan. Second, we fix the laser energy and only the energy of the electron beam is tuned during this scan. The two cases are called the tunable and fixed cases, respectively.

Table 1. The statistical errors of the SM Higgs boson mass by devoting $50/10 \text{ fb}^{-1}$ to each point. The results in the parentheses are calculated with the tagging efficiencies 70% and 3.5% of $b\bar{b}(g)$ and $c\bar{c}(g)$ events, respectively.

$m_{h\text{SM}}$ (GeV)	$\Delta m_{h\text{SM}}$ (MeV)					
	80	90	100	110	120	140
Tunable case	+140	+120	+100 (+140)	+140	+170	+210
	-150	-140	-110 (-160)	-100	-100	-220
Fixed case	+140	+120	+100 (+190)	+170	+200	+220
	-170	-130	-120 (-160)	-110	-130	-270

Table 2. The statistical errors of the total width of the SM Higgs boson by devoting 50/10 fb^{-1} to each point. The results in the parentheses are calculated with the tagging efficiencies 70% and 3.5% of $b\bar{b}(g)$ and $c\bar{c}(g)$ events, respectively.

$m_{h_{\text{SM}}}$ (GeV)	$\Delta\Gamma_h/\Gamma_{h_{\text{SM}}}$ (%)					
	80	90	100	110	120	140
Tunable case	+7.8	+6.7	+6.0 (+7.8)	+5.7	+5.7	+7.5
	-7.0	-6.1	-5.6 (-6.9)	-5.3	-5.6	-6.8
Fixed case	+8.5	+7.3	+6.6 (+8.5)	+6.2	+6.3	+8.1
	-7.6	-6.6	-6.0 (-7.5)	-5.7	-5.8	-7.3

Table 1 lists the statistical errors of the SM Higgs boson mass at the 1σ level, using an integrated luminosity of 50/10 fb^{-1} . In this table, the mass errors of the tunable case are almost smaller than those of the fixed case. Since the background processes $\gamma\gamma \rightarrow q\bar{q}(g)$ are increasing at the lower Higgs mass and the branching ratio $B(h \rightarrow b\bar{b})$ is decreasing at the higher Higgs mass, the errors of the Higgs boson mass near 100 GeV are the smallest. The statistical errors $\sqrt{S+B}/S$ of the total width $\Gamma_h/\Gamma_{h_{\text{SM}}}$ of the SM Higgs boson with a 50 fb^{-1} luminosity are listed in Table 2. The statistical errors of the total width for intermediate-mass Higgs bosons are almost within 8% in Table 2. Comparatively the results with the tagging efficiencies 70% and 3.5% of $b\bar{b}(g)$ and $c\bar{c}(g)$ events are listed in Tables 1 and 2.

Table 3. The expected precision for the mass of the Higgs boson with $m_{h_{\text{SM}}} = 100$ GeV at the future colliders.^{1,2} The NLC threshold result is at $\sqrt{s} = m_Z + m_{h_{\text{SM}}} + 0.5$ GeV including the initial state radiation and the beam energy spread.² The LHC error is for ATLAS+CMS.¹ The error at the muon collider is devoted to the scan with beam energy resolution of 0.01%.¹

	NLC (threshold)	LHC	Muon Collider	Photon-Photon Collider
$\Delta m_{h_{\text{SM}}}$ (MeV)	60	95	0.1	110 (90)
Luminosity (fb^{-1})	100	600	200	50 (100)

At the future colliders, the expected precision for the mass of the Higgs boson with $m_{h_{\text{SM}}}=100$ GeV is listed in Table 3. The NLC threshold result is at $\sqrt{s} = m_Z + m_{h_{\text{SM}}} + 0.5$ GeV including the initial state radiation and the beam energy spread.² The LHC error is for ATLAS+CMS including the statistical and systematic errors.¹ The error at the muon collider is devoted to the scan with beam energy resolution of 0.01%.¹ From the table, the accuracy of the Higgs boson mass at the muon collider is the highest, however the systematic error at the muon collider is neglected assuming accurate beam energy determination. The accuracy at the photon-photon collider is 1.5 times lower than that at the NLC threshold case. Therefore we can perform the complementary measurement of Higgs boson mass at photon-photon colliders.

As for other origins of the errors, we need to know the systematic uncertainties on the luminosity distribution. The possibilities of the luminosity measurements at photon-photon colliders have been studied using the process $\gamma\gamma \rightarrow l^+l^-$ or $\gamma\gamma \rightarrow$

W^+W^- .^{15,17} For energy scanning the measurement of the luminosity distribution at the high energy-edge is crucial and we need to study it further.

5. Summary

In this paper, we have shown that it is possible to determine the Higgs boson mass to a high precision by the method of energy scanning at photon-photon colliders, using the high energy edge of the photon spectrum.

Acknowledgments

I express sincere thanks to T. Takahashi, T. Tauchi, V. Telnov, I. Watanabe, M. Xie and K. Yokoya for useful discussions.

References

1. J.F. Gunion *et al.*, in *Proceedings of the 1996 DPF/DPB Summer Study on New Directions for High-Energy Physics (Snowmass, 96)*, Snowmass, CO, June 25-July 12, 1996, p.541.
2. V. Barger, M.S. Berger, J.F. Gunion, and T. Han, Phys. Rev. Lett. **78**, 3991 (1997).
3. V. Barger, M.S. Berger, J.F. Gunion, and T. Han, Phys. Rept. **286**, 1 (1997).
4. I.F. Ginzburg, G.L. Kotkin, V.G. Serbo, and V.I. Telnov, Nucl. Instrum. and Methods **205**, 47 (1983); A **219**, 5 (1984).
5. V. Telnov, Nucl. Instrum. and Methods Phys. Res. A **355**, 3 (1995).
6. V. Telnov, in *Proceedings of the 2nd International Workshop on Electron-Electron Interactions at TeV Energies*, Santa Cruz, CA, Sep 22-24, 1997, Int. J. Mod. Phys. A **13**, 2399 (1998).
7. D.L. Borden, D.A. Bauer, and D.O. Caldwell, SLAC-PUB-5715, 1992.
8. D.L. Borden, D.A. Bauer, and D.O. Caldwell, Phys. Rev. D **48**, 4018 (1993).
9. D.L. Borden, V.A. Khoze, W.J. Stirling, and J. Ohnemus, Phys. Rev. D **50**, 4499 (1994).
10. G. Jikia and A. Tkabladze, Phys. Rev. D **54**, 2030 (1996).
11. T. Ohgaki, T. Takahashi, and I. Watanabe, Phys. Rev. D **56**, 1723 (1997).
12. M. Melles and W.J. Stirling, Phys. Rev. D **59**, 094009 (1999); Eur. Phys. J C **9**, 101 (1999); DTP-98-100 (1998); M. Melles, W.J. Stirling, and V.A. Khoze, DTP-99-70 (1999).
13. D.J. Jackson, Nucl. Instrum. Meth. A **388** 247 (1997).
14. LCFI Collaboration, P.N. Burrows *et al.*, in *Proceedings of the 8th International Workshop on Vertex Detectors (Vertex 99)*, Texel, Netherlands, June 20-25, 1999.
15. I. Watanabe *et al.*, Report No. KEK-97-17, 1998.
16. A. Djouadi, J. Kalinowski, and M. Spira, Comput. Phys. Commun. **108**, 56 (1998).
17. Y. Yasui, I. Watanabe, J. Kodaira, and I. Endo, Nucl. Instrum. and Methods Phys. Res. A **335**, 385 (1993).